

Article

Not peer-reviewed version

A Novel Platinum Modified Barium Zirconate-Based Electrolyte for Enhanced Solid Oxide Fuel Cell Performance

[Yonghong Liu](#) , [Min Fu](#) ^{*} , Jiarou Liu , Yuxin Zhang , [Zetian Tao](#)

Posted Date: 21 November 2023

doi: 10.20944/preprints202311.1350.v1

Keywords: proton-conducting solid oxide fuel cells; electrolyte; conductivity; electrochemical performance



Preprints.org is a free multidiscipline platform providing preprint service that is dedicated to making early versions of research outputs permanently available and citable. Preprints posted at Preprints.org appear in Web of Science, Crossref, Google Scholar, Scilit, Europe PMC.

Copyright: This is an open access article distributed under the Creative Commons Attribution License which permits unrestricted use, distribution, and reproduction in any medium, provided the original work is properly cited.

Article

A Novel Platinum Modified Barium Zirconate-Based Electrolyte for Enhanced Solid Oxide Fuel Cell Performance

Yonghong Liu ¹, Min Fu ^{2,*}, Jiarou Liu², Yuxin Zhang ² and Zetian Tao ²

¹ College of Safety Science & Engineering, Liaoning Technical University, Huludao 125105, China

² School of Resources, Environment and Safety Engineering, University of South China, Hengyang, Hunan Province 421001, China

* Correspondence: fu_min@stu.usc.edu.cn

Abstract: Pt modified BaZr_{0.76}Y_{0.2}Ni_{0.04}O₃ (BZYN) is fabricated and characterized as a stable electrolyte for proton-conducting solid oxide fuel cell (H-SOFC). The utilization of X-ray diffraction method (XRD) and transmission electron microscopy (TEM) enables the identification of the presence of platinum (Pt) in both the crystal lattice sites and the grain interface. This occurrence contributes to a reduction in grain boundary resistance. Consequently, this phenomenon improves the conductivity of the electrolyte. The electrochemical performance of the single cell with Pt modified BZY electrolyte is improved by the reduction of ohmic resistance and enhancement of ion migration. This signifies a noteworthy advancement in the creation of more efficient and durable proton-conducting SOFCs.

Keywords: proton-conducting solid oxide fuel cells; electrolyte; conductivity; electrochemical performance

1. Introduction

The past few decades have witnessed a persistent rise in interest in proton solid oxide fuel cells (H-SOFCs) due to the pressing demand for clean energy and environmental conservation. The primary reason for their suitability for future commercial applications is their excellent cell performance and better conversion efficiency at intermediate temperatures[1]. Barium cerate and barium zirconate materials exhibit a notable degree of proton mobility, rendering them highly suitable as electrolytes for H-SOFCs. This is mostly attributed to their exceptional proton conductivity[2–4]. The currently predominant proton-conducting oxides in use are materials based on BaCeO₃. These materials have notable ionic conductivity, but are prone to chemical instability when exposed to atmospheres containing CO₂ and H₂O. [5,6]. Yttrium-doped BaCeO₃ has superior proton conductivity compared to other oxides within its class. However, its commercial viability is hindered by insufficient chemical stability when subjected to operational conditions within a cell[4,7].

In recent years, researchers have made significant progress in developing viable techniques to address the challenges associated with BaZrO₃ based materials, thereby enhancing their suitability for use in proton conducting SOFCs. Considering the chemical stability, fabrication feasibility and proton conductivity, Y doped BaZrO₃ (BZY) shows promising application potential[8–10]. Although the bulk proton conductivity of BZY is competitive with other proton conductors, the high grain boundary resistance caused by its poor sintering ability hinders widely application as an electrolyte for H-SOFCs[11]. In recent years, numerous endeavors have been undertaken to enhance the sintering density of BZY, hence reducing the resistance at grain boundaries[12,13]. Sintering aids, such as zinc oxide (ZnO) and nickel oxide (NiO), are employed to lower sintering temperatures. Extensive study has been conducted to investigate the underlying mechanisms by which these aids exert control over stoichiometry. It is found that NiO can react with BZY and BaZr_{0.76}Y_{0.2}Ni_{0.04}O₃

(BZYN) exhibits adequate total conductivity. Hence, it is imperative to investigate a viable approach for the production of high-performance BZY cells without the intentional inclusion of sintering aids, since this offers significant benefits for practical application.

Platinum (Pt) is frequently employed as the electrode material for conducting conductivity tests, as well as serving as an electrode in fuel cell testing[14,15]. The experimental procedure for evaluating the electrochemical properties of BZY material involves several stages. Firstly, a dense BZY pellet is prepared through the process of sintering. Subsequently, a layer of Pt film is applied onto the surface of the dense BZY pellet. Finally, the coated pellet is subjected to high-temperature firing to serve as the electrodes for testing the electrochemical properties. The potential interaction between Pt and BZY is often overlooked since Pt is considered an inert substance. Bi has recently provided a definitive result regarding the diffusion of Pt into the lattice of BZY[16]. Another study indicates that at elevated temperatures, Pt has the potential to undergo a reaction with BaCeO_3 , resulting in the formation of different proton conductor phases [17]. It follows that Pt is not totally inert with proton-conducting oxides, and that a reaction will take place between Pt and BZY. In addition, the reaction of Pt and BZY powders is also studied and O1s binding energy decreases which might be crucial to proton migration[18]. On account of the demands of proton-conducting electrolytes, it is imperative to elucidate the impact of Pt on conductivity and boundary resistance.

In the present work, we chose BZYN as electrolyte which was treated with Pt foil at the high sintering temperature. The influence of Pt on the phase structure, grain boundary growth, and electrical conductivity of the materials were investigated. In addition, an anode-supported fuel cell with Pt modified BZYN electrolyte was assembled and its performance was evaluated to determine the benefits of employing this approach for H-SOFCs.

2. Experimental

2.1. Materials Synthesis

BZYN powders were produced via a wet chemical combustion method supported by citric acid[19]. The appropriate weights of several raw precursors were identified based on the stoichiometric ratio derived from the BZYN formula. Initially, appropriate precursors of BaCO_3 (99.95%, Macklin), $\text{Zr}(\text{NO}_3)_4 \cdot 5\text{H}_2\text{O}$ (99.99%, Macklin), $\text{Y}(\text{NO}_3)_3 \cdot 6\text{H}_2\text{O}$ (99.99%, Macklin), and $\text{Ni}(\text{NO}_3)_2 \cdot 6\text{H}_2\text{O}$ (Xilong Scientific) were dissolved into dilute nitric acid solution while Citric acid monohydrate (99.99%, Macklin) with a weight ratio of 1.5:1 to metallic ions was added as complexing agents. Afterwards, the pH of the solution was modulated to around 7 using ammonia, resulting in a transparent solution. Following that, the solution endured continuous mixing at a temperature of 80 °C until combustion, which was subsequently subjected to firing at a temperature of 1000 °C for 3 h.

2.2. Characterization and Electrochemical Measurement

The BZYN powders were pressed under 300MPa to form BZYN pellets which were subsequently sintered at 1550 °C for 10h for the electrical conductivity test. The sintered pellets were treated on Pt foil at 1300 °C for 5 h to obtain Pt modified BZYN (Pt-BZYN). The total electrical conductivities of the sintered pellets were measured by analyzing impedance spectrum via a Zahner Zennium electrochemical workstation with amplitude of 5 mV.

The BZYN electrolyte was co-pressed on the anode substrate and functional layer mezzanine. The anode powder is composed of BZYN, NiO and starches in a ratio of 40: 60: 20, while the functional layer powder is formed of BZYN and NiO in a ratio of 45:55. The functional layer powder synthesized by BaCO_3 (99.95%, Macklin), $\text{Zr}(\text{NO}_3)_4 \cdot 5\text{H}_2\text{O}$ (99.99%, Macklin), $\text{Y}(\text{NO}_3)_3 \cdot 6\text{H}_2\text{O}$ (99.99%, Macklin), and $\text{Ni}(\text{NO}_3)_2 \cdot 6\text{H}_2\text{O}$ (Xilong Scientific) by the wet chemical combustion method with the assistance of citric acid. The half-cell was then sintered at 1350 °C for 5 h. Pt-BZYN electrolyte was obtained through placing previous BZYN powder on the surface of Pt foil and heating it at 1000 °C for 3 h. Powdered $\text{La}_{0.6}\text{Sr}_{0.4}\text{Co}_{0.2}\text{Fe}_{0.8}\text{O}_{3-\delta}$ (LSCF) was combined with 10 wt% of ethylcellulose-pineol adhesive to create the cathode slurry. The BZYN and Pt-BZYN electrolytes were then screen printed with the cathode

slurry before being calcined at 1000 °C for 3 h. Subsequently, the cell performance was measured between 600 to 700 °C on an electrochemical workstation (Admiral-plus-1772). Wet hydrogen gas, containing about 3% water, was used as the fuel source at a flow rate of 25 ml min⁻¹ while ambient air was adopted as oxidant. The Linear Sweep Voltammetry (LSV) mode was employed to obtain the I-V/I-P curves of the cell. Furthermore, the Electrochemical Impedance Spectra (EIS) were obtained by conducting measurements under open circuit conditions. The frequency range utilized for these measurements was set at 0.1-1 MHz, while the alternating current (AC) amplitude was maintained at 10 mV.

The crystal phase and structure parameters of the produced BZYN and BZYNP samples were determined using X-ray diffraction (XRD) analysis, employing CuK α radiation. The morphology and elemental distribution of the powders were observed and analyzed through scanning electron microscopes (SEM, Phenom XL) and Transmission electron microscopy (TEM, JEOL JEM-F200).

3. Results and Discussion

Figure 1 presents XRD patterns of synthesized BZYN and Pt-BZYN powders. The image illustrates that only peaks attributed to BZYN and Pt-BZYN are present, indicating that both BZYN and Pt-BZYN exhibit a singular phase that can be identified as a cubic perovskite structure (PDF No. 06-0399). In order to observe the influence of Pt, an enlarged diffraction pattern is provided. Based on the observed specific magnification ranging from 26-34° in Figure 1, it is evident that the peaks exhibit a minor shift towards higher angles. In accordance with the Bragg equation, it becomes evident that the introduction of Pt as a dopant leads to a reduction in the lattice constants. This phenomenon can be attributed to the variance in atomic radius between Pt⁴⁺ (0.62 Å) and Zr⁴⁺ (0.79 Å), resulting in a reduction of the lattice parameter when Zr⁴⁺ is replaced with Pt⁴⁺.

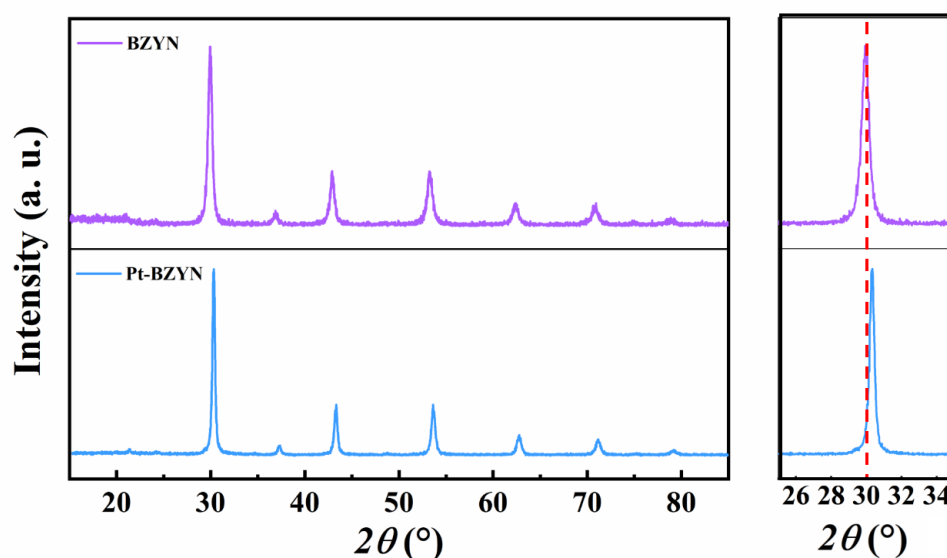


Figure 1. XRD patterns of as-prepared BZYN and Pt-BZYN mixture after co-fired at temperature of 1000°C for 3h.

The microstructures of the sintered Pt-BZYN samples were meticulously examined using scanning electron microscopy (SEM) and are prominently displayed in Figure 2(a). Notably, the sample exhibits a state of complete density, devoid of any discernible pores. This compelling observation underscores that the introduction of Pt as a dopant has no adverse effects on the sintering activity. In addition, energy dispersive spectroscopy (EDS) is employed to investigate the elemental distribution within the material, and these results are thoughtfully illustrated in Figure 2(b-f). The elemental analysis reveals a remarkably even dispersion of Ba, Y, Ni, and Zr throughout the sample.

Interestingly, minute quantities of Pt are also detectable. This distribution pattern of Pt strongly suggests its potential incorporation into the BZYN lattice, consistent with the previously discussed XRD findings.

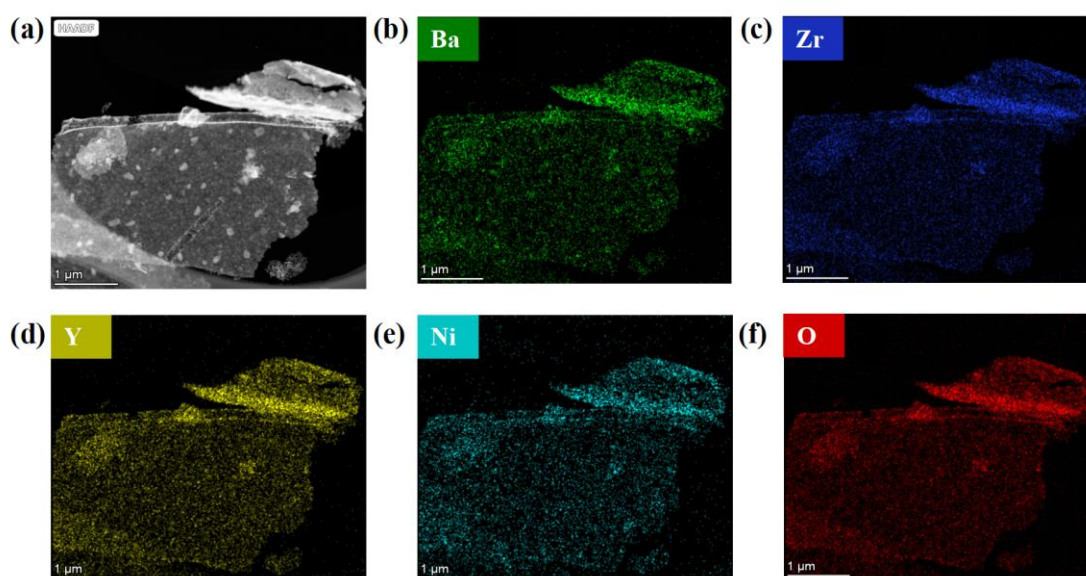


Figure 2. SEM-EDS elemental mapping of Pt, Zr, Ba, Y, Ni and O.

Through a meticulous analysis of lattice parameters and structural characteristics, it has been unequivocally demonstrated that Pt not only partially inhabits the lattice sites but also conforms to findings in the existing literature on this subject [20]. In our study, to further study doping sites of Pt, the morphology of Pt-BZYN powders are characterized using transmission electron microscopy (TEM). Figure 3(d) illustrates the presence of dark nano-particles attached to the grain boundary, indicating that Pt has a tendency to aggregate at the interface in addition to occupying lattice sites. This aggregation of Pt on the grain boundary may have a positive impact on ion conductivity. It is because the resistance at the grain boundary significantly influences the conductivity of BZY. In addition, it is obvious from Figure 3(c) that a d-spacing value of 0.300 nm corresponds to (110) planes of BaZrO₃-based material as reported by reference[21]. Conversely, a d-spacing value of 0.21 nm corresponds to the (110) planes of Pt-based materials, as depicted in Figure 3(b)[22,23]. This compelling evidence confirms the presence of Pt generated at the grain boundaries. Furthermore, Figure 4 presents the transmission electron microscopy-energy dispersive X-ray spectroscopy (TEM-EDX) scanning outcome of Pt-BZYN, providing insights into the quantification of platinum (Pt) content within the Pt-BZYN samples.

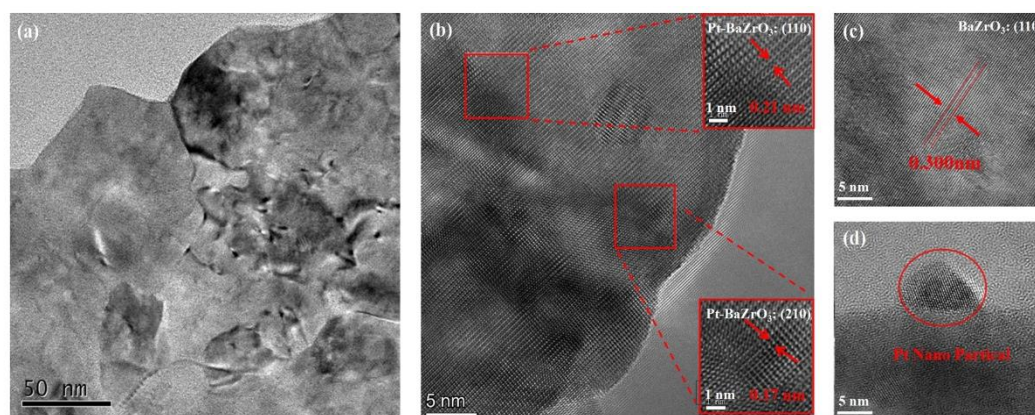


Figure 3. TEM image displayed d-spacing of BaZrO₃-based material and Pt.

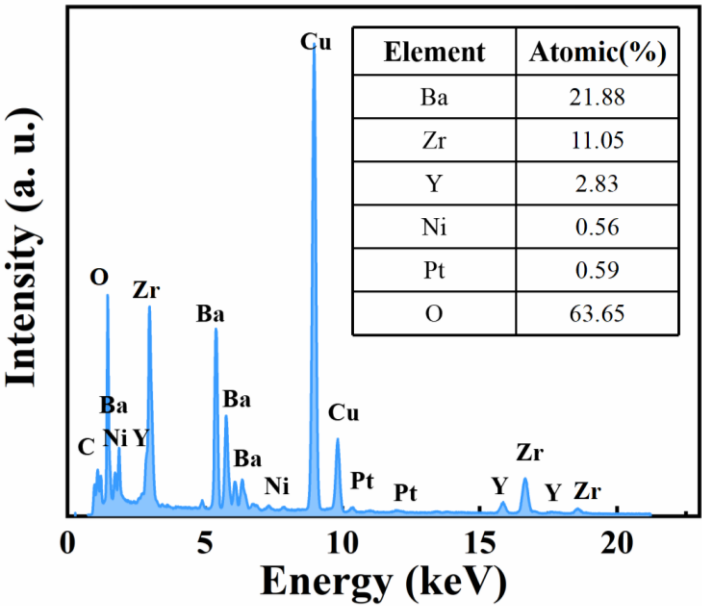


Figure 4. TEM-EDX scanning result of Pt-BZYN.

The conductivity of BZYN and Pt-BZYN was meticulously assessed under ambient air at various temperatures via electrochemical impedance spectroscopy, and the results are visually presented in Figure 5. It becomes readily apparent that Pt-BZYN consistently exhibits notably higher conductivities across the temperature range of 350°C to 700°C, in sharp contrast to BZYN. This conspicuous difference underscores the critical role of Pt doping in enhancing conductivity, a factor that exhibits a direct and positive correlation with electrochemical performance.

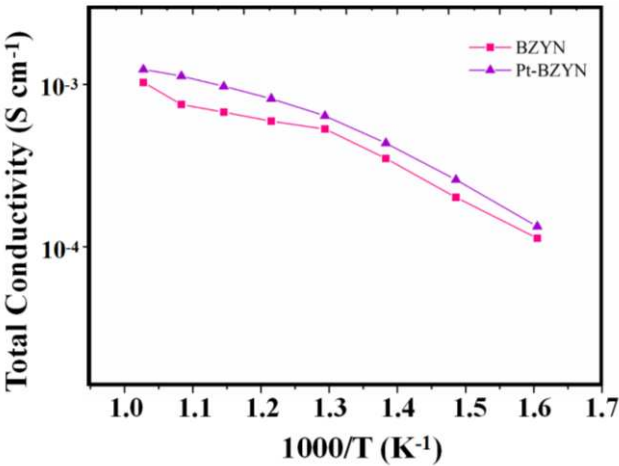


Figure 5. Total conductivity curves of fuel cells with different electrolyte membranes of Pt-BZYN, BZYN measured at different temperatures from 350 °C to 700 °C.

The cross-sectional microstructure of single cells utilizing BZYN and Pt-BZYN as the electrolyte materials is vividly illustrated in Figure 6. This micrograph reveals four distinct layers, with the electrolyte layer boasting a thickness of approximately 6-7 micrometers. Furthermore, it's evident that both electrolyte layers exhibit a high degree of density, signifying robust contact between the electrolytes and electrodes, thus ensuring the integrity of the hydrogen containment within the cell. Given the uniformity in electrolyte thickness, the electrochemical performances of these assembled

single cells are characterized and evaluated. Figure 7a presents a compelling comparison of the cell performance of H-SOFCs employing BZYN and Pt-BZYN electrolytes at an operating temperature of 700 °C. Clearly, the cell with Pt-BZYN as the electrolyte exhibits superior performance. Notably, there is an approximate 15% enhancement in maximum power density (MPD) observed, rising from 350 to 408 mW·cm⁻². In Figure 7c, we can observe the cell performance of Pt-BZYN at various temperatures, revealing a positive correlation between power density and operating temperatures. Specifically, as depicted in the figure, the MPDs achieved are 408 mW cm⁻² at 700°C, 345 mW cm⁻² at 650°C, and 290 mW cm⁻² at 600°C for the single cell. This trend underscores the significance of temperature control in optimizing power density in the cell.

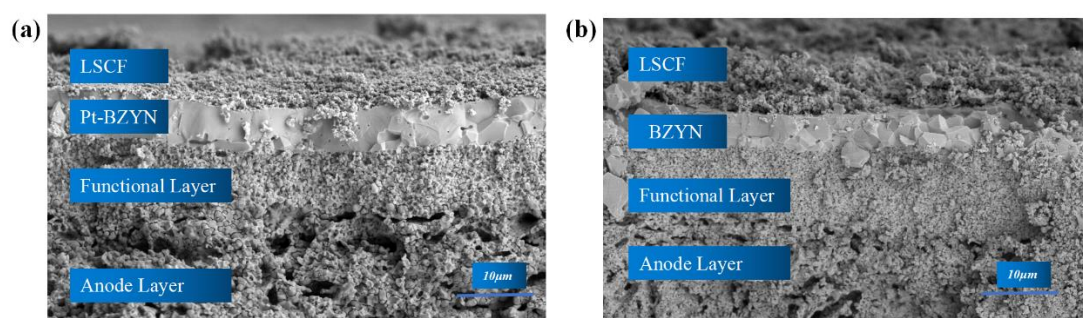


Figure 6. SEM micrographs of the fuel cell cross-sections and electrolyte membrane for (a) BZYN, (b) Pt-BZYN.

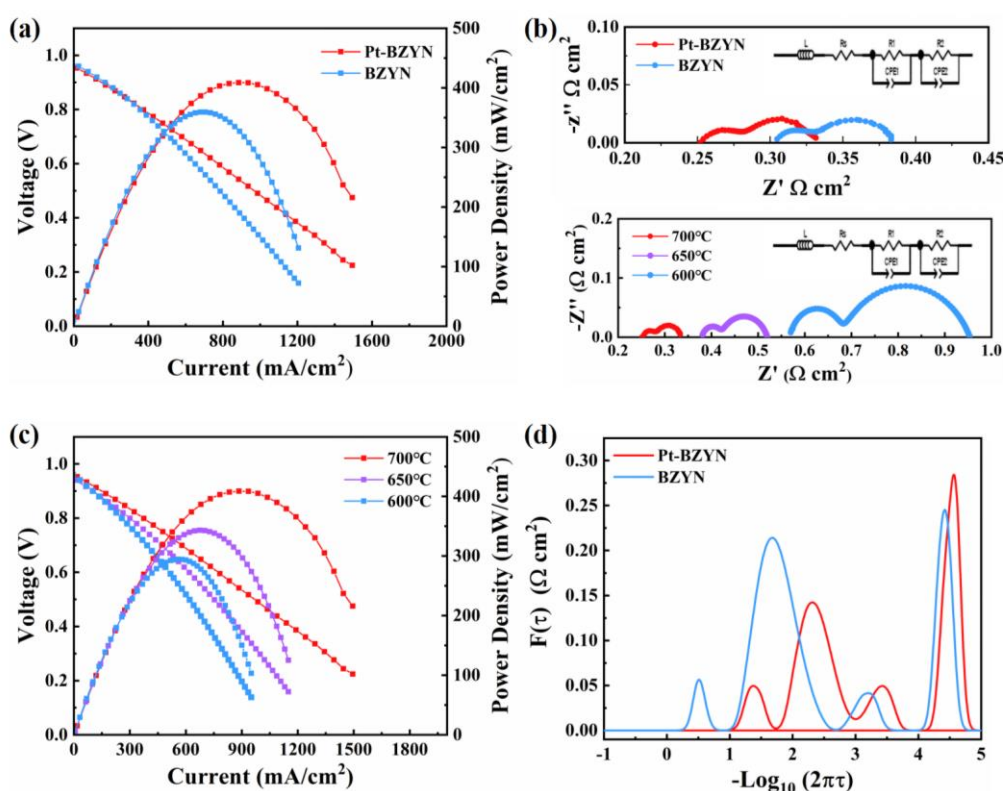


Figure 7. (a) I-V and power density curves for the cell with Pt-BZYN, BZYN electrolyte membrane measured at 700 °C; (b) A comparison of impedance plots of fuel cells with BZYN and Pt-BZYN electrolyte membrane measured at 700 °C and impedance plots of fuel cells with Pt-BZYN electrolyte membrane measured at 600, 650, and 700 °C.; (c) I-V and power density curves for the cell with Pt-

BZYN electrolyte membrane measured at 600, 650, and 700 °C ; (d) The impedance spectra corresponding distributions of relaxation times plots for the fuel cells with different electrolyte membrane.

The electrochemical impedance spectra (EIS) of the cells under open circuit voltage (OCV) conditions were conducted to assess the impact of Pt. As illustrated in Figure 7b, it can be observed that the polarization resistance (R_p) values of the two different cells are nearly identical. This suggests that the electrolyte has a relatively weak influence on R_p , with the main factors potentially being related to the cathode materials and their structures. However, it is clear that the ohmic resistance of Pt-BZYN is much lower than that of BZYN, indicating the conductivity of the electrolyte is improved through doping of Pt which in turn modifies the grain boundary to decrease grain boundary resistance. Furthermore, the EIS results across the temperature range from 600 °C to 700 °C are presented. As illustrated, the overall ohmic resistance decreases from 0.56 $\Omega \text{ cm}^2$ at 600 °C to 0.25 $\Omega \text{ cm}^2$ at 700 °C, indicating a negative relationship between temperature and ohmic resistance. Additionally, there are two distinct arcs in the impedance spectrum, corresponding to the two cathode reaction processes related to oxygen adsorption and transmission.

Recently, the distribution of relaxation time (DRT) method has been employed for analyzing EIS results to gain insights into the detailed reaction processes of fuel cells. In Figure 7(d), we present the DRT results calculated from impedance spectra obtained at 700 °C to investigate the impact of Pt. Notably, there are several distinct peaks, each representing specific reaction processes. The peaks at high and low frequencies are relatively similar, while the peak at intermediate frequency shows significant differences. It's worth highlighting that the process at intermediate frequency is influenced by the migration of protons and oxygen ions [24]. The higher conductivity associated with Pt likely facilitates greater proton transfer to the cathode side through the electrolyte, thereby reducing the intensity of the peak at the intermediate frequency.

4. Conclusion

The low conductivity of BZYN due to the high grain boundary resistance hindered its application as a stable electrolyte for H-SOFCs. A simple technique via volatilization of platinum was adopted to treat BZYN electrolyte. The XRD results showed that Pt modified BZYN had the same phase structure as BZYN and lattice parameters decreased for the lower ion radius, presenting Pt partially located into the lattice sites. TEM results further determined that nanoparticle of Pt attached at the grain boundary which may be beneficial for the ion conductivity. The cell with Pt-BZYN electrolyte displayed a higher maximum power density of 408 mW cm^{-2} and a lower polarization resistance of 0.25 $\Omega \cdot \text{cm}^2$ compared to the cell employing BZYN as electrolyte at 700 °C. Our findings suggest that the application of Pt treatment can be considered as a viable and efficient technical approach.

Acknowledgments: This work was supported by the National Natural Science Foundation of China (Grant Nos.: 11875164) and Natural Science Foundation of the Higher Education Institutions of Jiangsu Province (No. 18KJA430017).

References

1. Gao, Y.; Zhang, M.; Fu, M.; Hu, W.; Tong, H.; Tao, Z., A comprehensive review of recent progresses in cathode materials for Proton-conducting SOFCs. *Energy Reviews* **2023**, 100038.
2. Loureiro, F. J.; Nasani, N.; Reddy, G. S.; Munirathnam, N.; Fagg, D. P., A review on sintering technology of proton conducting BaCeO₃-BaZrO₃ perovskite oxide materials for Protonic Ceramic Fuel Cells. *Journal of Power Sources* **2019**, 438, 226991.
3. Vignesh, D.; Sonu, B. K.; Rout, E., Factors constituting proton trapping in BaCeO₃ and BaZrO₃ perovskite proton conductors in fuel cell technology: a review. *Energy & Fuels* **2022**, 36, (14), 7219-7244.
4. Tong, H.; Fu, M.; Yang, Y.; Chen, F.; Tao, Z., A Novel Self-Assembled Cobalt-Free Perovskite Composite Cathode with Triple-Conduction for Intermediate Proton-Conducting Solid Oxide Fuel Cells. *Advanced Functional Materials* **2022**, 32, (48), 2209695.

5. Dudek, M.; Lis, B.; Lach, R.; Daugela, S.; Salkus, T.; Kezionis, A.; Mosialek, M.; Socha, R. P.; Morgiel, J.; Gajek, M.; Sitarz, M.; Ziabka, M., $\text{Ba}_{0.95}\text{Ca}_{0.05}\text{Ce}_{0.9}\text{Y}_{0.1}\text{O}_3$ as an electrolyte for proton-conducting ceramic fuel cells. *Electrochimica Acta* **2019**, 304, 70-79.
6. Xie, K.; Yan, R. Q.; Liu, X. Q., Stable $\text{BaCe}_{0.7}\text{Ti}_{0.1}\text{Y}_{0.2}\text{O}_{3-\delta}$ proton conductor for solid oxide fuel cells. *Journal of Alloys and Compounds* **2009**, 479, (1-2), L40-L42.
7. Hossain, M. K.; Iwasa, T.; Hashizume, K., Hydrogen isotope dissolution and release behavior in Y-doped BaCeO_3 . *Journal of the American Ceramic Society* **2021**, 104, (12), 6508-6520.
8. Han, D.; Uda, T., The best composition of an Y-doped BaZrO_3 electrolyte: selection criteria from transport properties, microstructure, and phase behavior. *Journal of Materials Chemistry A* **2018**, 6, (38), 18571-18582.
9. Fluri, A.; Marcolongo, A.; Roddatis, V.; Wokaun, A.; Pergolesi, D.; Marzari, N.; Lippert, T., Enhanced proton conductivity in Y-doped BaZrO_3 via strain engineering. *Advanced Science* **2017**, 4, (12), 1700467.
10. Hu, H. J.; Zou, J.; Shan, L.; Jiang, X. Q.; Ni, Y. J.; Li, X. B.; Qian, X. W.; Chen, W. W.; Zhou, Y. C.; Zhang, W. F.; Wei, S. H.; Jian, J. W., Conductivities in Yttrium-Doped Barium Zirconate: A First-Principles Study. *Crystals* **2023**, 13, (3).
11. Bondevik, T.; Bjørheim, T. S.; Norby, T., Assessing common approximations in space charge modelling to estimate the proton resistance across grain boundaries in Y-doped BaZrO_3 . *Physical Chemistry Chemical Physics* **2020**, 22, (21), 11891-11902.
12. Sun, W.; Zhu, Z.; Shi, Z.; Liu, W., Chemically stable and easily sintered high-temperature proton conductor $\text{BaZr}_{0.8}\text{In}_{0.2}\text{O}_{3-\delta}$ for solid oxide fuel cells. *Journal of power sources* **2013**, 229, 95-101.
13. Sun, W.; Shi, Z.; Liu, M.; Bi, L.; Liu, W., An easily sintered, chemically stable, barium zirconate-based proton conductor for high-performance proton-conducting solid oxide fuel cells. *Advanced Functional Materials* **2014**, 24, (36), 5695-5702.
14. Ji, S.; Tanveer, W. H., Thickness determination of porous Pt cathode thin film capped by atomic layer-deposited alumina for low-temperature solid oxide fuel cells. *Applied Surface Science* **2020**, 514.
15. Gandavarapu, S. R.; Sabolsky, K.; Gerdes, K.; Sabolsky, E. M., Direct foamed and nano-catalyst impregnated solid-oxide fuel cell (SOFC) cathodes. *Materials Letters* **2013**, 95, 131-134.
16. Xu, Y. S.; Kou, H. N.; Fang, S. H.; Wang, X. F.; Bi, L., Evaluation of potential reaction between $\text{BaZr}_{0.8}\text{Y}_{0.2}\text{O}_{3-\delta}$ ceramics and Pt at high temperatures. *Ceramics International* **2019**, 45, (17), 22383-22387.
17. Lussier, J. A.; Shafi, S. P.; Donaberger, R. L.; Bieringer, M., Platinum Uptake and $\text{Ba}_2\text{CePtO}_6$ Formation During in Situ $\text{BaCe}_{1-x}\text{M}_x\text{O}_{3-\delta}$ ($\text{M}=\text{La}, \text{In}$) Formation. *Inorganic Chemistry* **2014**, 53, (16), 8809-8815.
18. Xu, Y.; Kou, H.; Fang, S.; Wang, X.; Bi, L., Evaluation of potential reaction between $\text{BaZr}_{0.8}\text{Y}_{0.2}\text{O}_{3-\delta}$ ceramics and Pt at high temperatures. *Ceramics International* **2019**, 45, (17), 22383-22387.
19. Fu, M.; Lin, X.; Li, X. Y.; Tao, Z. T., Applications of microwave technology in the field of solid oxide fuel cell - a review. *Russian Chemical Reviews* **2023**, 92, (9).
20. Xu, Y.; Kou, H.; Fang, S.; Wang, X.; Bi, L., Evaluation of potential reaction between $\text{BaZr}_{0.8}\text{Y}_{0.2}\text{O}_{3-\delta}$ ceramics and Pt at high temperatures. *Ceramics International* **2019**, 45, (17), 22383-22387.
21. Shi, N.; Xie, Y.; Huan, D.; Yang, Y.; Xue, S.; Qi, Z.; Pan, Y.; Peng, R.; Xia, C.; Lu, Y., Controllable CO_2 conversion in high performance proton conducting solid oxide electrolysis cells and the possible mechanisms. *Journal of Materials Chemistry A* **2019**, 7, (9), 4855-4864.
22. Mohamed, R. M.; Ismail, A. A.; Kadi, M. W.; Alresheedi, A. S.; Mkhaliid, I. A. J. A. o., Fabrication of mesoporous PtO-ZnO nanocomposites with promoted photocatalytic performance for degradation of tetracycline. **2021**, 6, (9), 6438-6447.
23. Zheng, L.; Xie, J.; Liu, X.; Yang, C.; Zheng, W.; Zhang, J. J. A. A. M.; Interfaces, Unveiling the electronic interaction in ZnO/PtO/Pt nanoarrays for catalytic detection of triethylamine with ultrahigh sensitivity. **2020**, 12, (41), 46267-46276.
24. Wang, X.; Ma, Z.; Zhang, T.; Kang, J.; Ou, X.; Feng, P.; Wang, S.; Zhou, F.; Ling, Y., Charge-transfer modeling and polarization DRT analysis of proton ceramics fuel cells based on mixed conductive electrolyte with the modified anode-electrolyte interface. *ACS applied materials & interfaces* **2018**, 10, (41), 35047-35059.

Disclaimer/Publisher's Note: The statements, opinions and data contained in all publications are solely those of the individual author(s) and contributor(s) and not of MDPI and/or the editor(s). MDPI and/or the editor(s) disclaim responsibility for any injury to people or property resulting from any ideas, methods, instructions or products referred to in the content.